

# Discovery of Novel Inhibitors of a Disintegrin and Metalloprotease 17 (ADAM17) Using Glycosylated and Non-glycosylated Substrates<sup>\*[5]</sup>

Received for publication, June 6, 2012, and in revised form, August 20, 2012. Published, JBC Papers in Press, August 27, 2012, DOI 10.1074/jbc.M112.389114

Dmitriy Minond<sup>1</sup>, Mare Cudic, Nina Bionda, Marc Giulianotti, Laura Maida, Richard A. Houghten, and Gregg B. Fields

From the Torrey Pines Institute for Molecular Studies, Port St. Lucie, Florida 34987

**Background:** Most reported ADAM17 inhibitors are zinc-binding and not selective.

**Results:** Novel selective ADAM17 inhibitors were discovered and characterized.

**Conclusion:** Novel ADAM17 inhibitors act via a non-zinc-binding mechanism.

**Significance:** Selective non-zinc-binding inhibitors of ADAM proteases can be useful research and therapeutic tools.

A disintegrin and metalloprotease (ADAM) proteases are implicated in multiple diseases, but no drugs based on ADAM inhibition exist. Most of the ADAM inhibitors developed to date feature zinc-binding moieties that target the active site zinc, which leads to a lack of selectivity and off-target toxicity. We hypothesized that secondary binding site (exosite) inhibitors should provide a viable alternative to active site inhibitors. Potential exosites in ADAM structures have been reported, but no studies describing substrate features necessary for exosite interactions exist. Analysis of ADAM cognate substrates revealed that glycosylation is often present in the vicinity of the scissile bond. To study whether glycosylation plays a role in modulating ADAM activity, a tumor necrosis factor  $\alpha$  (TNF $\alpha$ ) substrate with and without a glycan moiety attached was synthesized and characterized. Glycosylation enhanced ADAM8 and -17 activities and decreased ADAM10 activity. Metalloprotease (MMP) activity was unaffected by TNF $\alpha$  substrate glycosylation. High throughput screening assays were developed using glycosylated and non-glycosylated substrate, and positional scanning was conducted. A novel chemotype of ADAM17-selective probes was discovered from the TPIMS library (Houghten, R. A., Pinilla, C., Giulianotti, M. A., Appel, J. R., Dooley, C. T., Nefzi, A., Ostresh, J. M., Yu, Y., Maggiora, G. M., Medina-Franco, J. L., Brunner, D., and Schneider, J. (2008) Strategies for the use of mixture-based synthetic combinatorial libraries. Scaffold ranking, direct testing *in vivo*, and enhanced deconvolution by computational methods. *J. Comb. Chem.* 10, 3–19; Pinilla, C., Appel, J. R., Borràs, E., and Houghten, R. A. (2003) Advances in the use of synthetic combinatorial chemistry. Mixture-based libraries. *Nat. Med.* 9, 118–122) that preferentially inhibited glycosylated substrate hydrolysis and spared ADAM10, MMP-8, and MMP-

14. Kinetic studies revealed that ADAM17 inhibition occurred via a non-zinc-binding mechanism. Thus, modulation of proteolysis via glycosylation may be used for identifying novel, potentially exosite binding compounds. The newly described ADAM17 inhibitors represent research tools to investigate the role of ADAM17 in the progression of various diseases.

A disintegrin and metalloprotease (ADAM)<sup>2</sup> proteases are implicated in multiple diseases, including but not limited to several types of cancer (3, 4), rheumatoid arthritis (5), and Alzheimer disease (6). Multiple clinical trials of small molecule inhibitors of the most studied ADAM protease, ADAM17, were discontinued due to toxicity (5, 7) as a result of the lack of selectivity of these inhibitors. Most of the ADAM inhibitors developed to date feature zinc-binding moieties that target the active site zinc (8). There are ~70 known human metalloproteases (ADAM, ADAMTS, and MMP) (9) that have zinc in their active site, which explains off-target toxicities of zinc-binding inhibitors (10).

Secondary binding site (exosite) inhibitors provide a viable alternative to active site inhibitors (11–16). Selective exosite inhibitors of MMP-13 that were discovered by several groups (17–21), including ours, are currently being investigated for arthritis therapy. Exosites are defined as sites outside of the active site that participate in substrate recognition and binding (11).

Enzymes from multiple families and classes have been shown to contain exosites: serine, cysteine, and metalloproteases (22–25), metallo- $\beta$ -lactamases (26), kinases (27), oxidoreductases (28), nucleases (29), and deacetylases (30). Moreover, non-zinc-binding exosite inhibitors were reported for MMP and ADAMTS proteases (17, 18, 22), which are closely related to ADAM proteases. Therefore, although currently there are only a few reports of potential exosites in ADAM protease structures

<sup>\*</sup> This work was supported, in whole or in part, by National Institutes of Health Grants 1R03DA033985-01 (to D. M.), CA098799 (to G. B. F.), and 1R01DA031370 (to R. A. H.). This work was also supported by James and Esther King Biomedical Research Program Grant 2KN05 (to D. M.), by the Multiple Sclerosis National Research Institute (to G. B. F.), and by the State of Florida, Executive Office of the Governor's Office of Tourism, Trade, and Economic Development.

<sup>[5]</sup> This article contains supplemental Materials and Methods.

<sup>1</sup> To whom correspondence should be addressed: Torrey Pines Institute for Molecular Studies, 11350 SW Village Pkwy., Port St. Lucie, FL 34987. Tel.: 772-345-4705; Fax: 772-345-3649; E-mail: dminond@tpims.org.

<sup>2</sup> The abbreviations used are: ADAM, a disintegrin and metalloprotease; ADAMTS, ADAM with thrombospondin motifs; MMP, metalloprotease; TFE, trifluoroethanol; TPIMS, Torrey Pines Institute for Molecular Studies; AHA, *N*-hydroxyacetamide; ECD, ectodomain; SAR, structure-activity relationship.

## Novel ADAM17 Inhibitors

(31, 32), it is likely that ADAM proteases possess exploitable exosites. A recent report by Tape *et al.* (33) demonstrated that it is possible to achieve selective binding to the ADAM17 ectodomain by an antibody that exploits exosites.

Substrate recognition by ADAM proteases is a largely unexplored area. Substrate specificity of closely related proteases from ADAMTS and MMP families was shown to be due to a combination of sequence features and substrate topology (34–37). Although cleavage site sequence specificity was addressed for several members of the ADAM family (38–40), there are no studies of the effects of secondary structure on substrate recognition by ADAM proteases.

Similarly, it is not known whether other substrate features, such as glycosylation, play a role in ADAM substrate specificity. Glycosylation was shown to cause peptides to assume a repertoire of different conformations (41, 42) due either to stabilization or destabilization of glycosylated structure as compared with a non-modified peptide (43, 44). Additionally, it was shown that the rate of enzymatic hydrolysis of glycosylated peptides was dependent on the distance of the glycosylation site from the scissile bond (45). This suggests the possibility of glycosylation serving as specific cleavage signal or, alternatively, an effect of different peptide conformations on enzyme hydrolytic activity.

ADAM substrates exhibit various degrees of glycosylation, whereas distances of glycosylation sites from respective scissile bonds also vary significantly. For example, the cleavage site of TNF $\alpha$  by ADAM17 is only four residues away from a glycosylated residue (46), whereas glycosylation occurs 14 residues away from the TGF $\alpha$  cleavage site (47) and more than 200 residues away from the L-selectin cleavage site (48).

In this work, we have investigated the role of glycosylation in the specificity of ADAM-catalyzed reactions using TNF $\alpha$  as a model substrate. Enzyme-substrate interactions based on glycosylation were subsequently utilized to identify novel, potentially exosite-binding ADAM17 inhibitors.

### EXPERIMENTAL PROCEDURES

**Substrate Synthesis, Purification, and Characterization**—Experimental details are listed in the supplemental materials. Briefly, substrate synthesis was performed on a Protein Technology PS3 peptide synthesizer using Fmoc (*N*-(9-fluorenyl)-methoxycarbonyl) solid-phase peptide chemistry methodology. Substrates were purified using reversed-phase HPLC. Fractions were analyzed by matrix-assisted laser desorption/ionization time-of-flight mass spectrometry (MALDI-TOF MS) and by analytical reversed-phase HPLC.

**Circular Dichroism Spectroscopy**—CD spectra were recorded over the range  $\lambda = 190$ –250 nm with a Jasco J-810 spectropolarimeter using a 0.2-cm path length quartz cell. Substrate solutions were prepared in deionized water. Raw CD data (millidegrees) was normalized for respective substrate concentrations to obtain molar ellipticity ( $\theta$ ) to allow for direct comparison of CD signatures of different substrates.

**Enzyme Kinetics**—ADAM and MMP enzymes were purchased from R&D Systems (Minneapolis, MN) with the exception of MMP-14, which was purchased from Millipore (Temecula, CA). ADAM8 and -12 were activated as per the

manufacturer's instructions. Active enzyme concentrations were determined as described elsewhere (40). Substrate stock solutions were prepared at various concentrations in R&D Systems recommended assay buffers. Assays were conducted by incubating a range of substrate concentrations (2–100  $\mu$ M) with various ADAM enzyme concentrations at 25 °C. Fluorescence was measured on a multimode microplate reader Synergy H4 (Biotek Instruments, Winooski, VT) using  $\lambda_{\text{ex}} = 360$  nm and  $\lambda_{\text{em}} = 460$  nm. Rates of hydrolysis were obtained from plots of fluorescence *versus* time, using data points from only the linear portion of the hydrolysis curve. The slope from these plots was divided by the fluorescence change corresponding to complete hydrolysis and then multiplied by the substrate concentration to obtain rates of hydrolysis in units of  $\mu$ M/s. Kinetic parameters were calculated by non-linear regression analysis using the GraphPad Prism version 5.01 suite of programs. ADAM and MMP substrate cleavage sites were established by MALDI-TOF MS.

**Library Screening**—Mixture libraries (1, 2) were solubilized in 3% DMSO/H<sub>2</sub>O and added to polypropylene 384-well plates (Greiner catalog no. 781280). ADAM10 and -17 glycosylated and non-glycosylated substrate assays followed the same general protocol. 5  $\mu$ l of 3 $\times$  enzyme solution (30 nM) in assay buffer (10 mM Hepes, 0.001% Brij-35, pH 7.5) were added to solid bottom white 384-well low volume plates (Nunc, catalog no. 264706). Next, 5  $\mu$ l of test compounds or pharmacological controls were added to corresponding wells. After a 30-min incubation at room temperature, the reactions were started by the addition of 5  $\mu$ l of 3 $\times$  solutions of the respective substrates (30  $\mu$ M). Fluorescence was measured every 30 min for 2 h using the multimode microplate reader Synergy H4 (Biotek Instruments, Winooski, VT) using  $\lambda_{\text{ex}} = 360$  nm and  $\lambda_{\text{em}} = 460$  nm. Rates of hydrolysis were obtained from plots of fluorescence *versus* time, and inhibition was calculated using rates obtained from wells containing substrates only (100% inhibition) and substrates with enzyme (0% inhibition). Three parameters were calculated on a per plate basis: (a) the signal-to-background ratio; (b) the coefficient for variation (equal to the (S.D./mean)  $\times$  100) for all compound test wells; and (c) the *Z'*-factor (18). The IC<sub>50</sub> value of the pharmacological control (*N*-hydroxy-1-(4-methoxyphenyl)sulfonyl-4-(4-biphenylcarbonyl)piperazine-2-carboxamide; Calbiochem catalog no. 444252) was also calculated to ascertain the assay robustness. Each mixture library was screened in triplicate at 0.33 mg/ml.

**Inhibition Kinetics**—Glycosylated substrate and ADAM17 working solutions were prepared in buffer containing 10 mM Hepes, 0.001% Brij-35, pH 7.5. All reactions were conducted in 384-white polystyrene well plates (Nunc, catalog no. 264706). Determinations of inhibition constants and modalities were conducted by incubating the range of glycosylated substrate concentrations (1–50  $\mu$ M) with 2.5 nM ADAM17 at room temperature in the presence of varying concentrations of inhibitors. Fluorescence was measured as described above. Rates of hydrolysis were obtained from plots of fluorescence *versus* time, using data points from only the linear portion of the hydrolysis curve.

All kinetic parameters were calculated using GraphPad Prism version 5.01 (GraphPad Software, Inc., La Jolla, CA). All

**TABLE 1**  
ADAM cognate human substrates and their cleavage and glycosylation sites

UniProt no.	Substrate	Cleavage site	Glycosylated residue	Distance from scissile bond (no. of residues)	Type of glycosylation	ADAM
P35070	Pro-BTC	CVVA <sup>31</sup> ↓ DGNS	Asn <sup>34</sup>	3	N-Linked (GlcNAc)	10
P01375	Pro-TNF $\alpha$	LAQA <sup>76</sup> ↓ VRSS	Ser <sup>80</sup>	4	O-Linked (GalNAc)	17
P02786	TRP1	ECER <sup>100</sup> ↓ LAGT	Thr <sup>104</sup> , Asn <sup>251</sup> , Asn <sup>317</sup> , Asn <sup>727</sup>	4 <sup>a</sup>	O-Linked (GalNAc)	17
P08887	IL6-R	LPVQ <sup>357</sup> ↓ DSSV	Asn <sup>55</sup> , Asn <sup>93</sup> , Asn <sup>221</sup> , Asn <sup>350</sup>	7 <sup>a</sup>	N-Linked (GlcNAc)	10/17
O14944	Pro-EPR	DNPR <sup>59</sup> ↓ VAQV	Asn <sup>17</sup>	12	N-Linked (GlcNAc)	17
Q99075	Pro-HB-EGF	RKVR <sup>62</sup> ↓ DLQE	Thr <sup>75</sup> , Thr <sup>85</sup>	13 <sup>a</sup>	O-Linked (GalNAc)	10/17
P01135	Pro-TGF $\alpha$	VAAA <sup>39</sup> ↓ VVSH	Asn <sup>25</sup>	14	N-Linked (GlcNAc)	17

<sup>a</sup> Distance from the closest glycosylated site is indicated in cases of multiple glycosylations.

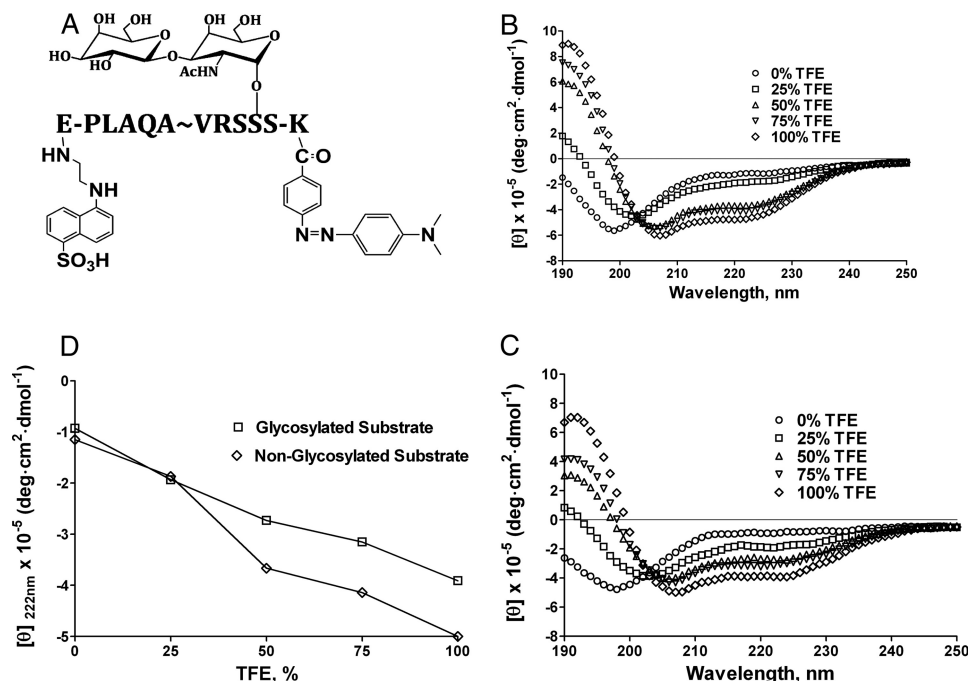


FIGURE 1. **Glycosylated substrate and substrate characterization by circular dichroism spectroscopy.** A, structure of glycosylated substrate (Glu(EDANS)-Pro-Leu-Ala-Gln-Ala-Val-Arg-Ser-Ser(TF)-Ser-Lys(DABCYL)). Shown are circular dichroism spectra of non-glycosylated (B) and glycosylated substrates (C). D, molar ellipticity of non-glycosylated and glycosylated substrates at  $\lambda = 222$  nm as a function of TFE concentration. TF, Thomsen-Freidenreich.

**TABLE 2**  
Kinetic parameters for ADAM hydrolysis of glycosylated and non-glycosylated substrates

Enzyme	$k_{cat}/K_m$		$k_{cat}$		$K_m$	
	Glycosylated	Non-glycosylated	Glycosylated	Non-glycosylated	Glycosylated	Non-glycosylated
	$M^{-1} s^{-1}$		$s^{-1}$		$\mu M$	
ADAM8	$1.4 \pm 0.1 \times 10^3$	$2.2 \pm 0.0 \times 10^2$	$0.04 \pm 0.01$	$0.01 \pm 0.03$	$31 \pm 11$	$46 \pm 15$
ADAM9	ND <sup>a</sup>	$1.2 \pm 0.1 \times 10^3$	ND	$0.06 \pm 0.01$	ND	$49 \pm 6$
ADAM10	$0.8 \pm 0.3 \times 10^4$	$2.5 \pm 0.7 \times 10^4$	$0.06 \pm 0.01$	$0.28 \pm 0.03$	$8.5 \pm 1.3$	$12 \pm 3$
ADAM12	$1.3 \pm 0.4 \times 10^3$	$8.5 \pm 0.5 \times 10^2$	$0.02 \pm 0.01$	$0.01 \pm 0.00$	$20 \pm 11$	$12 \pm 1$
ADAM17	$7.6 \pm 1.7 \times 10^4$	$1.2 \pm 0.1 \times 10^4$	$0.25 \pm 0.03$	$0.14 \pm 0.01$	$3.0 \pm 0.5$	$12 \pm 3$

<sup>a</sup> ND, not determined due to low reaction velocity.

$K_i$  and  $K'_i$  values were determined by non-linear regression (hyperbolic equation) analysis using the mixed inhibition model, which allows for simultaneous determination of mechanism of inhibition (13). The mechanism of inhibition was determined using the "alpha" parameter derived from a mixed model inhibition by GraphPad Prism. The mechanism of inhibition was additionally confirmed by Lineweaver-Burk plots.

**Dual Inhibition Kinetics**—A matrix of two different inhibitor combinations was created in 384-white polystyrene well plates (Nunc, catalog no. 264706) by serially diluting inhibitors in buffer containing 10 mM Hepes, 0.001% Brij-35, pH 7.5. ADAM17 ectodomain and glycosylated substrate were then

added resulting in 2.5 nM and 10  $\mu M$  final assay concentrations, respectively. Fluorescence was measured by a Synergy H4 (Biotek Instruments, Winooski, VT) using  $\lambda_{ex} = 360$  nm and  $\lambda_{em} = 460$  nm. Rates of hydrolysis were obtained from plots of fluorescence versus time, using data points from only the linear portion of the hydrolysis curve.

Initial rates of glycosylated substrate hydrolysis in the presence of two inhibitors were arranged as Yonetani-Theorell plots with  $1/v_{ij}$  plotted as a function of [I] in the presence of varying concentrations of inhibitor J. In Yonetani-Theorell plots, the intersecting lines indicate simultaneous (*i.e.* mutually non-exclusive) binding of both inhibitors to the enzyme (49, 50).

**TABLE 3**

Kinetic parameters for MMP hydrolysis of glycosylated and non-glycosylated substrates

Enzyme	$k_{cat}/K_m$		$k_{cat}$		$K_m$	
	Glycosylated	Non-glycosylated	Glycosylated	Non-glycosylated	Glycosylated	Non-glycosylated
	$M^{-1} s^{-1}$		$s^{-1}$		$\mu M$	
MMP-1	$1.1 \pm 0.1 \times 10^3$	$1.6 \pm 0.0 \times 10^3$	$0.03 \pm 0.02$	$0.02 \pm 0.00$	$12 \pm 0.2$	$12 \pm 0.0$
MMP-2	$0.4 \pm 0.7 \times 10^4$	$0.7 \pm 0.0 \times 10^4$	$0.02 \pm 0.01$	$0.02 \pm 0.01$	$5.9 \pm 0.6$	$2.8 \pm 0.6$
MMP-8	$1.1 \pm 0.1 \times 10^4$	$1.3 \pm 0.2 \times 10^4$	$0.2 \pm 0.03$	$0.3 \pm 0.2$	$17 \pm 2.5$	$13 \pm 1.3$
MMP-9	$1.9 \pm 0.2 \times 10^3$	$1.2 \pm 0.1 \times 10^3$	$0.01 \pm 0.00$	$0.01 \pm 0.00$	$7.4 \pm 2.1$	$7.3 \pm 2.7$
MMP-13	$1.7 \pm 0.2 \times 10^4$	$1.7 \pm 0.0 \times 10^4$	$0.1 \pm 0.04$	$0.07 \pm 0.02$	$6.8 \pm 3$	$4.4 \pm 0.9$
MMP-14	ND <sup>a</sup>	ND	ND	ND	ND	ND

ND, not determined.

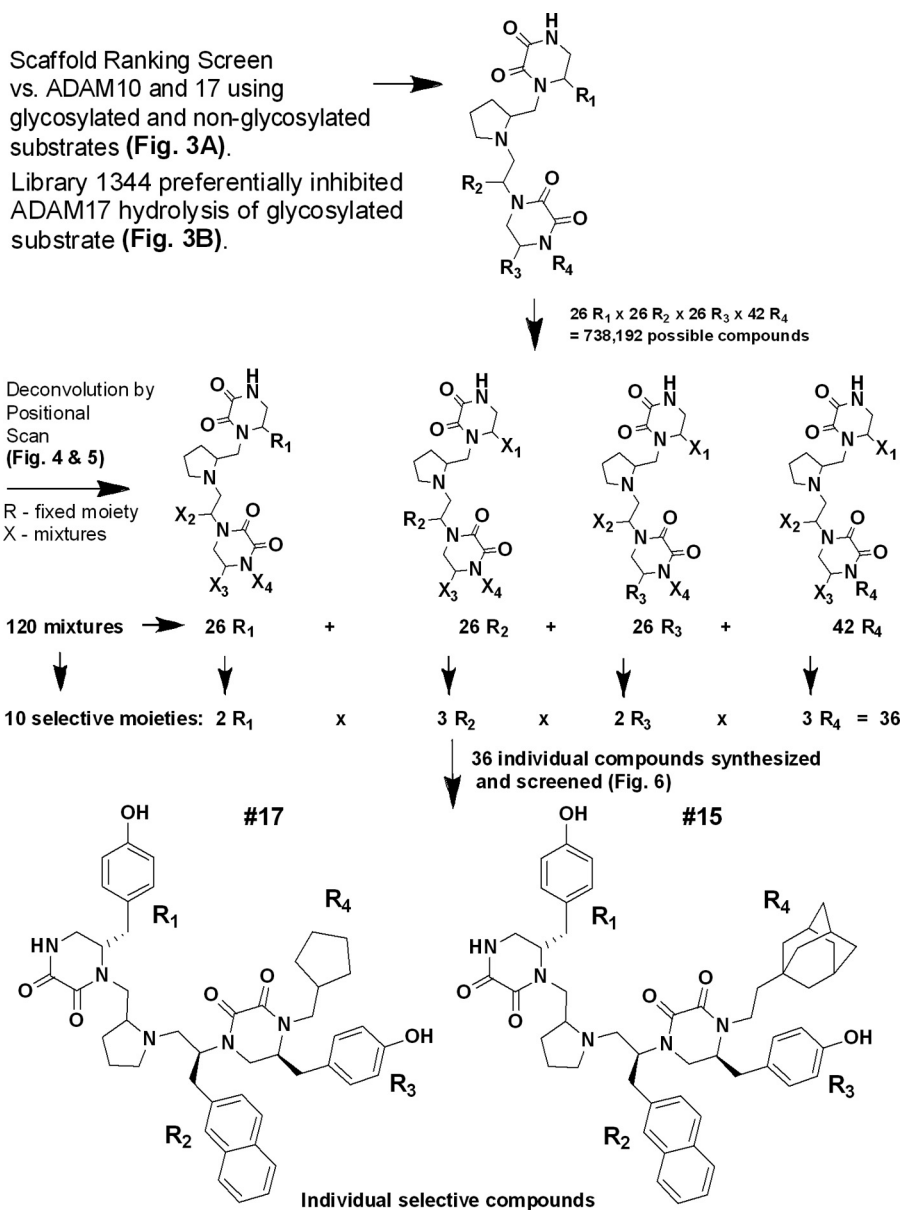


FIGURE 2. Summary of screening of TPIMS library for selective inhibitors of ADAM17.

**RESULTS AND DISCUSSION**

**Database and Literature Searches**—To determine which structural features of ADAM substrates can play a role in enzyme recognition and specificity, we examined the cognate human substrates of ADAM proteases. Overall, more than 30 ADAM substrates were analyzed. The analysis revealed that

several confirmed physiological substrates of ADAM proteases are post-translationally modified in the vicinity of the scissile bond. For example, pro-TNF $\alpha$  was reported to be O-glycosylated at Ser<sup>80</sup> in human B-cell lymphoblastic leukemia cells (BALL-1) (46). The mucin type 2,3- and 2,6-sialylated and non-sialylated core 1 structure ( $\beta$ -Gal-(1 $\rightarrow$ 3)-GalNAc), also known

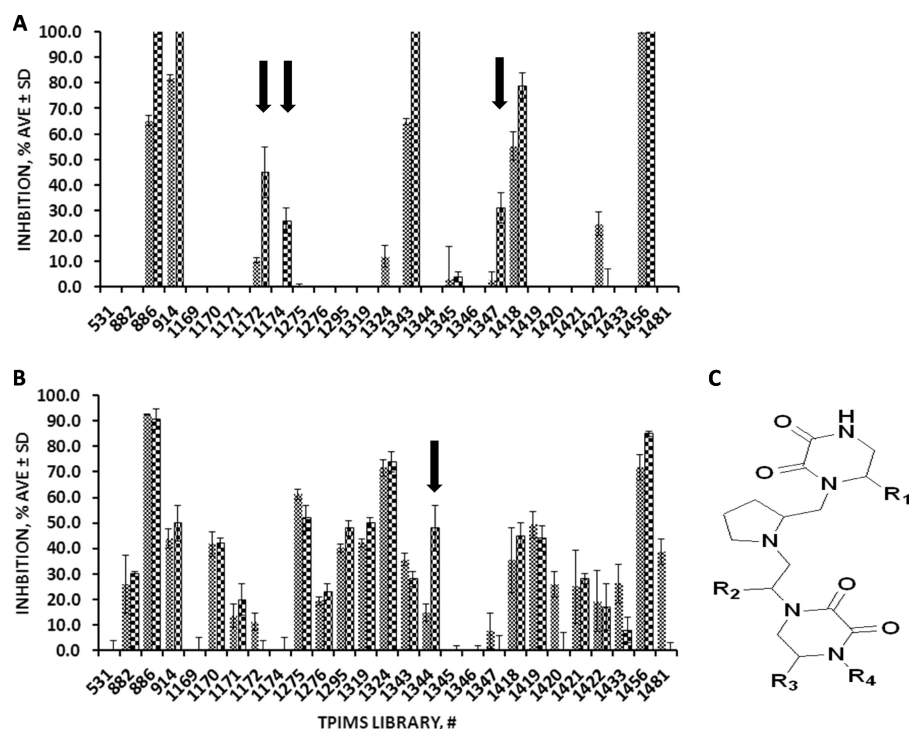


FIGURE 3. Results of the pilot “scaffold ranking” screen of TPIMS drug-like library against ADAM10 and 17. Shown is an ADAM10 (A) and ADAM17 (B) screen using glycosylated (checked bars) and non-glycosylated substrate (small checked bars). The arrows indicate libraries containing potential exosite inhibitors of ADAM10 and 17. All assays were performed in triplicate. Activity and selectivity of all libraries were confirmed in reversed-phase HPLC-based assays. (C), basic scaffold of library 1344.

as T- or TF-antigen, were identified. The physiological cleavage site by ADAM17 is at the Ala<sup>76</sup> ↓ Val bond, only 4 residues away from the modified Ser residue (Table 1). IL6-R (interleukin-6 receptor), which is cleaved by both ADAM10 and -17 (38, 51), was reported to be *N*-glycosylated by *N*-acetylglucosamine (GlcNAc) at four different positions (52, 53). Glycosylated Asn<sup>350</sup> is only 7 residues away from the Gln<sup>357</sup> ↓ Asp scissile bond (Table 1).

We hypothesized that the proximity of the carbohydrate moiety to the scissile bond of ADAM protease cognate substrates can have an effect on ADAM activity and, therefore, on production of soluble forms of cell surface molecules. To test this hypothesis, we synthesized substrates based on the cleavage site within TNF $\alpha$  (PLAQA<sup>76</sup> ↓ VRSSS) with and without TF-antigen (Fig. 1A) and characterized these substrates by circular dichroism spectroscopy and in enzymatic assays.

**Circular Dichroism Spectroscopic Analysis**—In order to determine the effect of glycosylation on substrate conformation and stability, CD spectra of non-glycosylated and glycosylated substrates in water and varying concentrations of TFE were recorded. CD spectra of 100% aqueous solution (0% TFE) and 25% TFE solutions of both non-glycosylated and glycosylated substrates exhibited characteristics of random coils featuring a single large negative peak at around  $\lambda = 198$  nm (Fig. 1, B and C). In the presence of high TFE concentrations (50–100%), both substrates exhibited spectra typical for an  $\alpha$ -helix with two minima at  $\lambda = 208$  and 222 nm. The plot of molar ellipticity at  $\lambda = 222$  nm as a function of TFE concentration (Fig. 1D) revealed that both substrates had similarly low  $\alpha$ -helical content at 0–25% TFE, whereas the non-glycosylated substrate had

a higher  $\alpha$ -helical content than the glycosylated substrate at 50–100% TFE.

The lower  $\alpha$ -helical content of glycosylated substrate compared with a non-glycosylated substrate at higher TFE concentrations is consistent with previous observations of the effects of *O*-glycosylation on peptide conformation (54, 55). This suggests that TF-antigen interferes with formation of the hydrogen bond pattern of an  $\alpha$ -helix, which is most likely attributable to steric hindrance. The calculated van der Waals volume of the Ser side chain is increased from 26.1 to 168.7 Å<sup>3</sup> due to the presence of a single carbohydrate moiety (56, 57).

**Substrate Cleavage Sites**—ADAM and MMP cleavage sites in glycosylated and non-glycosylated substrates were identified. ADAM10 and -17 cleaved only at the Ala ↓ Val bond in both substrates. ADAM8 also cleaved only the Ala ↓ Val bond of the non-glycosylated substrate but was able to cleave three different bonds (Ala ↓ Val, Gln ↓ Ala, and Val ↓ Arg) in the glycosylated substrate. ADAM12 cleaved at two positions of the non-glycosylated substrate (Ala ↓ Val and Gln ↓ Ala) and three positions in the case of the glycosylated substrate (Ala ↓ Gln, Gln ↓ Ala, and Val ↓ Arg). ADAM9 cleaved only at the Ala ↓ Val bond of the non-glycosylated substrate, but because there was very little hydrolysis of the glycosylated substrate, the exact cleavage site was not determined.

In the case of MMPs and the non-glycosylated substrate, the number and position of cleavage sites varied widely. MMP-1 and MMP-9 cleaved mainly at the Ala ↓ Val bond with secondary cleavage sites at Ala ↓ Gln (MMP-1 and MMP-9) and Arg ↓ Ser (MMP-1 only). In contrast, MMP-2 and MMP-13 cleaved at three different positions. MMP-2 had two major

## Novel ADAM17 Inhibitors

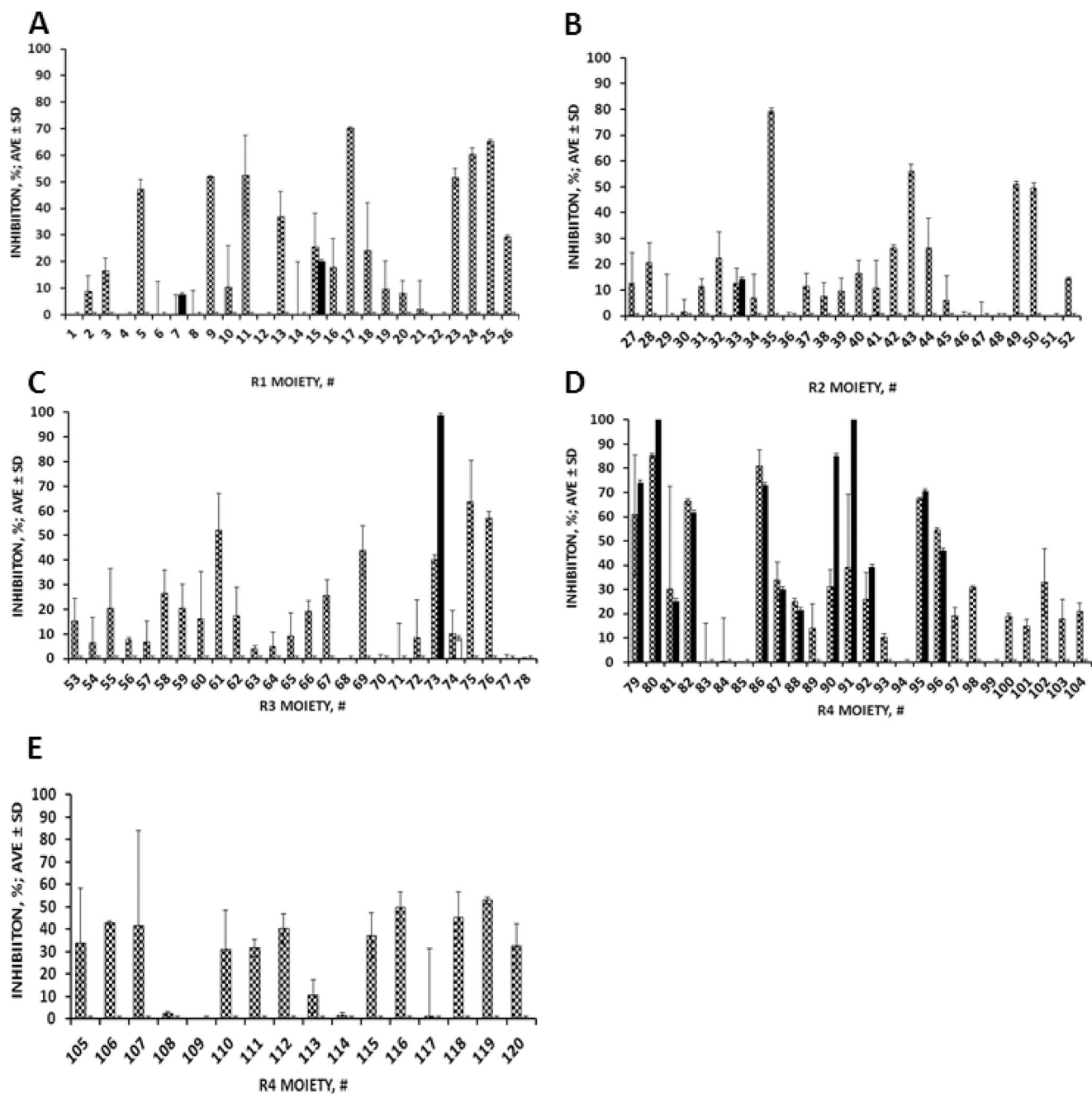


FIGURE 4. Results of the positional scan analysis of library 1344 against ADAM10 and -17. Positional scan of R<sub>1</sub> (A), R<sub>2</sub> (B), R<sub>3</sub> (C), and R<sub>4</sub> (D and E) defined moieties against ADAM10 (black bars) and ADAM17 (checked bars) using glycosylated substrate.

(Ala ↓ Val and Ser ↓ Ser) and one minor (Arg ↓ Ser) cleavage site, whereas MMP-13 appeared to cleave three positions (Ala ↓ Val, Ala ↓ Gln, and Val ↓ Arg) at the same rate. MMP-8 was able to hydrolyze the Ala ↓ Val bond only, thus exhibiting the most similarity with ADAM proteases.

Interestingly, in the presence of TF-antigen, all tested MMPs cleaved equally at just two positions (Ala ↓ Val and Gln ↓ Ala). Overall, only the ADAM10 and -17 cleavage site specificity was not affected by the presence of a carbohydrate moiety at the Ser<sup>80</sup> residue.

**Enzyme Kinetics**—In order to quantify the effect of glycosylation on ADAM proteolysis, kinetic parameters for hydrolysis of glycosylated and non-glycosylated substrates were deter-

mined. The  $K_m$  value for ADAM17 hydrolysis of the non-glycosylated substrate (Table 2) was in line with the published  $K_m$  value of  $19 \pm 5 \mu\text{M}$  (58). ADAM8 and -17 exhibited higher activity toward the glycosylated substrate as evidenced by 16- and 6-fold higher  $k_{\text{cat}}/K_m$  values, respectively (Table 2). The ADAM12  $k_{\text{cat}}/K_m$  value was slightly increased for the glycosylated substrate (Table 2). In the case of ADAM17, the increase in activity was due to the cumulative effects of changes in both  $K_m$  and  $k_{\text{cat}}$ , whereas ADAM8 improvement of activity was almost entirely due to an increase in  $k_{\text{cat}}$ . ADAM10 activity toward the glycosylated substrate was ~3-fold lower than for the non-glycosylated substrate due to a change in  $k_{\text{cat}}$  rather than  $K_m$ , which suggests that ADAM10 can accommodate the

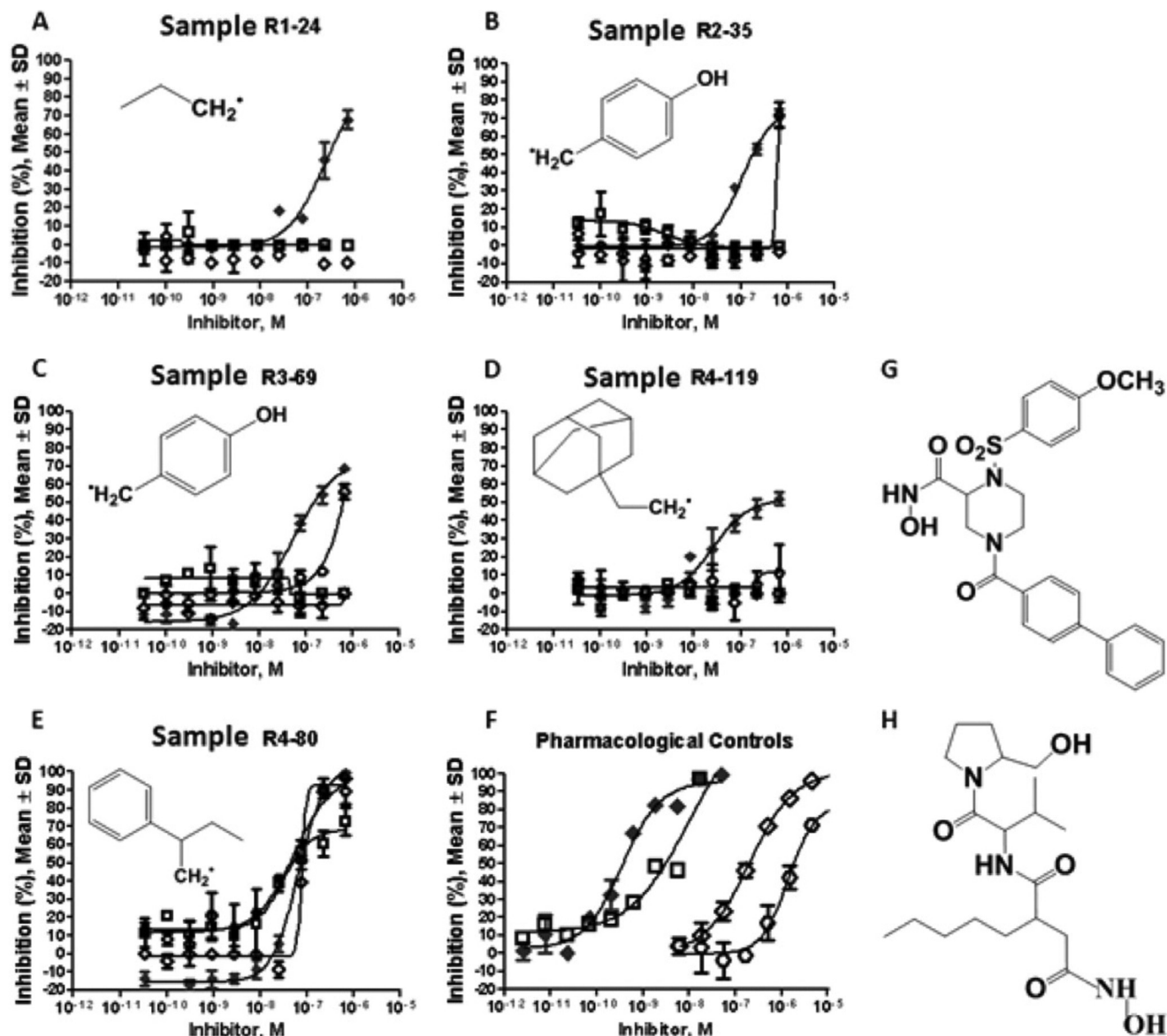


FIGURE 5. Results of dose-response study of most ADAM17-selective and potent mixture samples for each defined R position against metalloprotease panel. Shown are test libraries (A–E) and pharmacological assay controls (F) against ADAM10 (□), ADAM17 (◆), MMP-8 (◇), and MMP-14 (○). Structures of functional groups present in the defined R position for each sublibrary are shown as insets. Structures of MMP-9/-13 inhibitor (G) and actinonin (H) are shown. Note that sample R<sub>2</sub>-35 (see Fig. 5B) exhibits inhibition of MMP-14 only at the highest dose tested (1 μM).

carbohydrate moiety without the loss of affinity, albeit not as well as ADAM17 (Table 2). Because the carbohydrate moiety is accommodated by ADAM10, it is reasonable to hypothesize that ADAM10 contains a site that can be explored for exosite inhibitor discovery. Kinetic parameters of ADAM9-catalyzed hydrolysis of the glycosylated substrate were not determined due to very low activity. Approximately 10% of substrate was converted after 24 h of incubation with 25 nM ADAM9. For comparison, 25 nM ADAM8 converted 10% of glycosylated substrate within 30 min.

In order to determine whether substrate glycosylation has an effect on MMP catalysis, we determined kinetic parameters for MMP hydrolysis of glycosylated and non-glycosylated substrates. Interestingly, all tested MMPs, with the exception of MMP-14, exhibited very similar kinetic parameters for hydrolysis of either substrate (Table 3). In the case of MMP-14, the

rate of hydrolysis of both substrates was significantly lower than for the rest of the tested MMPs, which made kinetic evaluation unfeasible.

ADAM10 and -17 comprise a separate branch of the ADAM phylogenetic tree (9). They share 39% sequence similarity, but despite this low homology, it has proved difficult to design an isoform-selective inhibitor of ADAM17 (8). This situation is partially complicated by the absence of a crystal structure of the ADAM10 catalytic domain, which would allow the evaluation of structural differences between ADAM10 and -17.

Our kinetic data suggest differences in ADAM10 and -17 substrate binding site(s) corresponding to the Ser residue in position P<sub>4</sub>' of the TNF $\alpha$ -based substrate. Existing structural and modeling studies reveal the presence of a large S<sub>3</sub>' cleft in the ADAM17 structure that can potentially accommodate a bulky disaccharide ( $\beta$ Gal-1,3- $\alpha$ GalNAc) (59–61). Alignment

TABLE 4

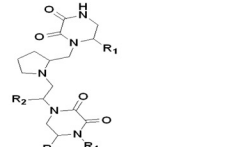
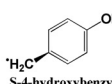
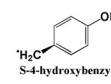
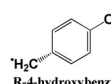
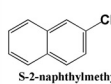
Most selective and potent functionalities against ADAM17 derived from positional scan of library 1344

Sample no.	Moieties in defined position			
	R <sub>1</sub>	R <sub>2</sub>	R <sub>3</sub>	R <sub>4</sub>
25	(S)-4-Hydroxybenzyl	Mix	Mix	Mix
24	(S)-Propyl	Mix	Mix	Mix
35	Mix	(S)-4-Hydroxybenzyl	Mix	Mix
43	Mix	(R)-4-Hydroxybenzyl	Mix	Mix
49	Mix	(S)-2-Naphthylmethyl	Mix	Mix
61	Mix	Mix	(S)-4-Hydroxybenzyl	Mix
69	Mix	Mix	(R)-4-Hydroxybenzyl	Mix
80	Mix	Mix	Mix	2-Phenylbutyl
119	Mix	Mix	Mix	2-Adamantan-1-yl-ethyl
106	Mix	Mix	Mix	Cyclopentyl-methyl

TABLE 5

SAR study results of individual compounds synthesized based on positional scan of 1344

Percentage inhibition data reported as a mean of three experiments  $\pm$  S.D.  $\mu$ M IC<sub>50</sub> values for the inhibition of ADAM17 are in parenthesis.

Sample #					Inhibition % @ 40 $\mu$ M			
	R <sub>1</sub>	R <sub>2</sub>	R <sub>3</sub>	R <sub>4</sub>	ADAM 10	ADAM 17	MMP 8	MMP 14
1			S-4-hydroxybenzyl	2-phenylbutyl	0	50 $\pm$ 2.5 (14)	0	19.8 $\pm$ 4.5
2			R-4-hydroxybenzyl		0	59 $\pm$ 0.3 (13)	0	15.6 $\pm$ 7.1
3			S-4-hydroxybenzyl	2-adamantan-1-yl-ethyl	0	56 $\pm$ 1.7 (6.4)	0	25.2 $\pm$ 2.8
4			R-4-hydroxybenzyl		0	60 $\pm$ 0.3 (7.7)	0	6 $\pm$ 8.2
5			S-4-hydroxybenzyl	cyclopentyl-methyl	0	34 $\pm$ 1 (>40)	0	19.3 $\pm$ 3.7
6			R-4-hydroxybenzyl		0	35 $\pm$ 0.3 (>40)	0	14.3 $\pm$ 3.1
7			2-phenylbutyl	S-4-hydroxybenzyl	0	58 $\pm$ 0.9 (18)	0	8.7 $\pm$ 2.6
8				R-4-hydroxybenzyl	0	53 $\pm$ 2.9 (24)	0	7.6 $\pm$ 1.5
9			S-4-hydroxybenzyl	2-adamantan-1-yl-ethyl	0	60 $\pm$ 0.9 (9.5)	0	1.3 $\pm$ 11
10			R-4-hydroxybenzyl		0	62 $\pm$ 0 (9.1)	1.1 $\pm$ 1.9	22.9 $\pm$ 13.2
11			S-4-hydroxybenzyl	cyclopentyl-methyl	0	38 $\pm$ 0.5 (>40)	2.1 $\pm$ 1.9	7.1 $\pm$ 0.8
12			R-4-hydroxybenzyl		0	42 $\pm$ 0.5 (>40)	0.9 $\pm$ 1.5	13.6 $\pm$ 3.5
13			2-phenylbutyl	S-4-hydroxybenzyl	0	54 $\pm$ 3 (6.2)	12 $\pm$ 1.6	19.9 $\pm$ 0.6
14				R-4-hydroxybenzyl	0	57 $\pm$ 0.3 (4.9)	9.3 $\pm$ 0	19.7 $\pm$ 7.2
15			S-4-hydroxybenzyl	2-adamantan-1-yl-ethyl	0	95 $\pm$ 0.2 (4.2)	12.9 $\pm$ 3.7	24.7 $\pm$ 0.1
16			R-4-hydroxybenzyl		0	61 $\pm$ 1.9 (4.4)	6.8 $\pm$ 7.8	22.4 $\pm$ 3.7
17			S-4-hydroxybenzyl	cyclopentyl-methyl	0	90 $\pm$ 2.2 (6.7)	0	18.3 $\pm$ 7.2
18			R-4-hydroxybenzyl		0	66 $\pm$ 4 (6.5)	2.1 $\pm$ 8.5	13.8 $\pm$ 7.9

of ADAM10 and -17 sequences shows that residues forming the ADAM17 S<sub>3</sub>' pocket are not conserved between ADAM10 and -17 (<sup>189</sup>EADLV *versus* <sup>189</sup>VSHIT for ADAM17 and -10, respectively) (60). Interestingly, the ADAM10 I192L/T193V double mutant cleavage specificity profile was indistinguishable from that of ADAM17 WT (38).

*Summary of Screening of Torrey Pines Institute for Molecular Studies (TPIMS) Library (Fig. 2)*—Primary screen (*Scaffold Ranking*) was conducted using 27 representative mixture libraries. Library 1344 was chosen for further studies (deconvolution by positional scanning). 120 mixture samples representative of library 1344 were screened first in single dose, and the 18 most active and selective mixture samples were screened in dose-response experiments against ADAM10 and -17 and MMP-8 and -14. Based on the most selective and active moieties in each defined R position, 36 individual compounds were synthesized and screened in dose-response experiments against ADAM10 and -17 and MMP-8 and -14.

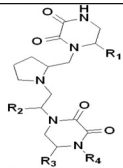

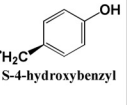
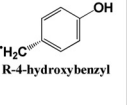
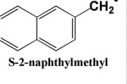
*Screening for Inhibitors of ADAM10 and -17 Using Glycosylated and Non-glycosylated Substrates*—Differences in kinetic parameters for ADAM17 hydrolysis of glycosylated and non-glycosylated substrates suggested that the carbohydrate moiety potentially interacts with hypothetical exosite and, therefore, could be exploited for inhibitor discovery. In order to test this hypothesis, high throughput screening assays were developed for ADAM10 and -17 using both glycosylated and non-glycosylated substrates. A pilot screen (termed the "scaffold ranking screen") was conducted for 27 mixture libraries representative of the TPIMS proprietary drug-like collection (1, 2). Parallel screens of libraries against ADAM10 and -17 yielded three libraries (Fig. 3A, compounds 1172, 1174, and 1347) preferentially inhibiting ADAM10 in the glycosylated substrate assay and one library (Fig. 3B, compound 1344) preferentially inhibiting ADAM17 in the glycosylated substrate assay, suggesting the possibility of the presence of exosite inhibitors in the above mentioned library mixtures. Most interestingly, the same



TABLE 6

SAR study results of individual compounds synthesized based on positional scan of 1344

Percentage inhibition data reported as a mean of three experiments  $\pm$  S.D.  $\mu\text{M}$   $\text{IC}_{50}$  values for the inhibition of ADAM17 are in parenthesis.

Sample #					Inhibition % @ 40 $\mu\text{M}$			
	R <sub>1</sub>	R <sub>2</sub>	R <sub>3</sub>	R <sub>4</sub>	ADAM 10	ADAM 17	MMP 8	MMP 14
19			S-4-hydroxybenzyl	2-phenylbutyl	0	31 $\pm$ 4.1 (>40)	0	2.3 $\pm$ 7.1
20			R-4-hydroxybenzyl	2-phenylbutyl	0	39 $\pm$ 5.7 (>40)	0	13.7 $\pm$ 5.2
21			S-4-hydroxybenzyl	2-adamantan-1-ylethyl	0	50 $\pm$ 4.1 (12)	1.3 $\pm$ 1	11.7 $\pm$ 0.8
22			R-4-hydroxybenzyl	2-adamantan-1-ylethyl	0	54 $\pm$ 1.5 (9.2)	2.4 $\pm$ 5.7	11.4 $\pm$ 1.4
23			S-4-hydroxybenzyl	cyclopentyl-methyl	0	18 $\pm$ 4.7 (>40)	0	0
24			R-4-hydroxybenzyl	cyclopentyl-methyl	0	17 $\pm$ 4.1 (>40)	0	3.4 $\pm$ 3
25			S-4-hydroxybenzyl	2-phenylbutyl	0	45 $\pm$ 0.6 (>40)	0	0
26			R-4-hydroxybenzyl	2-phenylbutyl	0	40 $\pm$ 3.9 (>40)	0	0
27			S-4-hydroxybenzyl	2-adamantan-1-ylethyl	0	60 $\pm$ 1.4 (12)	0	0
28			R-4-hydroxybenzyl	2-adamantan-1-ylethyl	0	59 $\pm$ 5 (5.7)	2.3 $\pm$ 0.4	4.9 $\pm$ 7.4
29			S-4-hydroxybenzyl	cyclopentyl-methyl	0	18 $\pm$ 4.1 (>40)	1.4 $\pm$ 2.6	2.1 $\pm$ 0.9
30			R-4-hydroxybenzyl	cyclopentyl-methyl	0	32 $\pm$ 0.1 (>40)	2.9 $\pm$ 4.8	11.3 $\pm$ 6.6
31		S-4-hydroxybenzyl	2-phenylbutyl	0	54 $\pm$ 2.4 (6.7)	8 $\pm$ 3.4	15.4 $\pm$ 0.5	
32		R-4-hydroxybenzyl	2-phenylbutyl	0	56 $\pm$ 0.1 (6.3)	9 $\pm$ 7	7.1 $\pm$ 7.4	
33		S-4-hydroxybenzyl	2-adamantan-1-ylethyl	0	51 $\pm$ 5 (8.3)	8.8 $\pm$ 4.5	18.8 $\pm$ 3.6	
34		R-4-hydroxybenzyl	2-adamantan-1-ylethyl	0	58 $\pm$ 8.4 (3.4)	9.8 $\pm$ 5.7	17.1 $\pm$ 5.3	
35		S-4-hydroxybenzyl	cyclopentyl-methyl	0	51 $\pm$ 2.4 (7.3)	7.9 $\pm$ 6.1	19 $\pm$ 0.1	
36		R-4-hydroxybenzyl	cyclopentyl-methyl	0	56 $\pm$ 6.9 (9.2)	10.5 $\pm$ 4.7	22.3 $\pm$ 1.2	

libraries were not active against ADAM10 and -17 in the non-glycosylated substrate assays and, therefore, would have been discarded from further studies if just the conventional active site-only substrate was utilized. Although not highly active against either target (maximum inhibition  $\leq$ 50%), these mixtures exhibited good selectivity, which, in combination with preferential inhibition of glycosylated substrate hydrolysis, suggests that these mixtures potentially inhibit ADAM10 and -17 via novel mechanisms. In order to confirm the selective profile of library 1344 (Fig. 3C), a structure-activity relationship study was conducted using a positional scan approach. A positional scan is a screen of a systematically formatted collection of compounds that allows for the rapid identification of the active functionalities around a core scaffold (1, 62).

The basic scaffold of library 1344 (Fig. 3C), composed of 738,192 ( $26 \times 26 \times 26 \times 42$ ) members, has four sites of diversity ( $R_1$ ,  $R_2$ ,  $R_3$ , and  $R_4$ ) and, therefore, is made up of four separate sublibraries, each having a single defined position (R) and three mixture positions (X). Screening the four sets of mixtures, totaling 120 mixtures ( $26 + 26 + 26 + 42$ ) against ADAM10 and -17 can provide information about the groups most important for activity and selectivity in each R position in library 1344 (1). Most of functional groups in positions  $R_1$ ,  $R_2$ , and  $R_3$  yielded libraries that either selectively inhibited ADAM17 or were inactive (Fig. 4, A–C). Functionalities in position  $R_4$  appear to influence the selectivity for ADAM17 to the greatest degree (Fig. 4, D and E). Approximately 50% of all substitutions tested in this position were inhibiting both enzymes to an equal extent.

We chose the library samples that were the most selective for and active against ADAM17 for each R position (total of 18)

to be studied in dose-response assays against ADAM10, ADAM17, MMP-8, and MMP-14. Additionally, we also chose  $R_4$ -80, which inhibited both ADAM10 and -17 equipotently (Fig. 4D), to act as a broad spectrum in-screen control. These samples exhibited 100–200 nM  $\text{IC}_{50}$  values against ADAM17 while sparing the three other metalloproteases (Fig. 5). To our knowledge, there are no publicly available selective ADAM17 inhibitors that spare ADAM10. In addition, these samples had little or no activity against MMP-8 and MMP-14, which are important anti-targets in skin and breast cancer (63–65). In contrast, sample  $R_4$ -80 exhibited a broad spectrum inhibition profile with  $\text{IC}_{50}$  values in the 100 nM range for all four metalloproteases tested (Fig. 5E), suggesting the importance of position  $R_4$  for selectivity among the metalloproteases. We used actinonin and MMP-9/-13 inhibitor as pharmacological assay controls for MMP-8 and MMP-14 and ADAM10 and -17, respectively (Fig. 5F). Both compounds are well known broad spectrum metalloprotease inhibitors (39, 40, 66, 67) that act via binding of the active site zinc. Based on the dose-response experiments with mixture libraries, we synthesized 36 individual compounds ( $2 R_1 \times 3 R_2 \times 2 R_3 \times 3 R_4$ ) containing functional groups for each defined R position that exhibited the most selectivity and potency toward ADAM17 (Table 4) and tested them against the target enzyme (ADAM17) and counter targets (ADAM10, MMP-8, and MMP-14) in a dose-response experiment. Only one of the 36 tested individual compounds (Tables 5 and 6) reached 25% inhibition at the highest tested concentration (40  $\mu\text{M}$ ) in the counter target assays (Table 5, sample 15), suggesting a highly selective nature of these compounds. The most active of the tested compounds had low

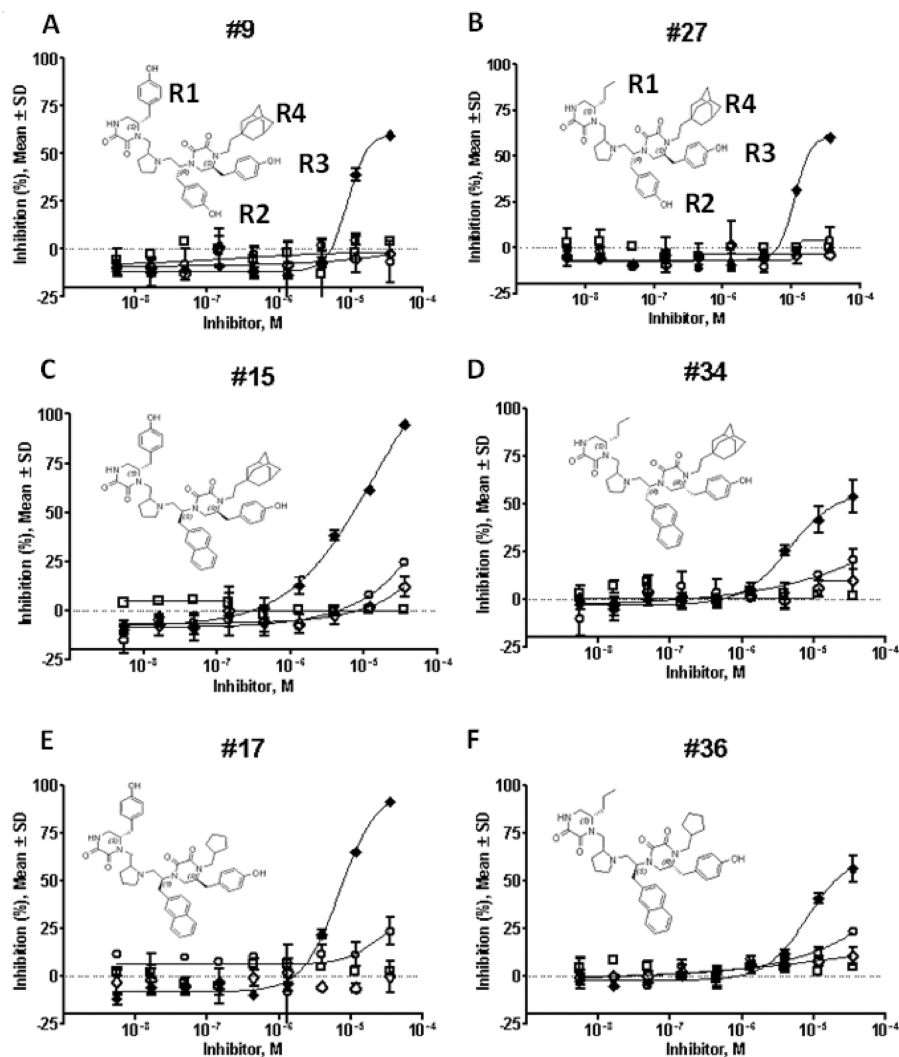


FIGURE 6. Results of dose response study of most ADAM17 selective and potent individual compounds. ADAM10 (□), ADAM17 (◆), MMP-8 (◇), and MMP-14 (○). Structures of individual compounds (compounds 9 (A), 27 (B), 15 (C), 34 (D), 17 (E), and 36 (F)) are shown as insets.

micromolar potency against ADAM17, whereas the mixture libraries had IC<sub>50</sub> values in 100 nM range.

According to the harmonic mean model (68), although mixture library 1344 has ~1000 individual constituents, the activity of the mixture can be attributed to the presence of one or few very potent compounds. Although we chose the functionalities for each R position that exhibited the most potency against ADAM17, it is entirely possible that the combination of these functionalities did not recapture the structure of the most potent individual constituent from each mixture library. Our future studies will therefore focus on the systematic iterative deconvolution of each position at a time.

**SAR Analysis**—Based on the positional scan of library 1344, position R<sub>1</sub> appears to be the most tolerant to the type of functionality present (Fig. 4A). The most active moieties are both aromatic (compound 5, (*S*)-phenyl; compound 9, (*R*)-2-naphthylmethyl; compound 25, (*S*)-4-hydroxybenzyl) and aliphatic (compound 13, (*S*)-isopropyl; compound 17, (*R*)-methyl; compound 23, (*R*)-cyclohexyl). Position R<sub>2</sub> has a strong preference for aromatic groups (compounds 35 and 43, (*S*)- and (*R*)-4-hydroxybenzyl; compounds 49 and 50, (*S*)- and (*R*)-naphthyl-

methyl) (Fig. 4B). Interestingly, (*S*)-4-hydroxybenzyl (compound 35) was preferred over (*R*)-4-hydroxybenzyl (compound 43), suggesting the importance of proper orientation of ligand in this binding site. Position R<sub>3</sub> exhibited preferences similar to R<sub>2</sub> (compounds 61 and 69, (*S*)- and (*R*)-4-hydroxybenzyl; compounds 75 and 76, (*S*)- and (*R*)-naphthylmethyl), suggesting the similarities between R<sub>2</sub> and R<sub>3</sub> binding sites within ADAM17 (Fig. 4C). The most potent substitutions in position R<sub>4</sub> were aromatic moieties (compounds 79, 80, 82, 86, 90, 91, 95, and 96; Fig. 4D), which, however, inhibited ADAM10 and -17 almost equipotently. In striking contrast, the most selective and potent ADAM17 substitutions were bulky cyclic aliphatic residues (compound 119, 2-adamantan-1-yl-ethyl; compound 116, 4-*tert*-butyl-cyclohexyl-methyl; compound 106, cyclopentyl-methyl).

Individual compounds synthesized on the basis of this positional scan analysis exhibited good selectivity for ADAM17. Both aromatic ((*S*)-4-hydroxybenzyl) and aliphatic ((*S*)-isopropyl) groups preserved ADAM17 selectivity when present in R<sub>1</sub> (Fig. 6, A and B, compounds 9 and 27). Substitution of the hydroxybenzyl of compound 9 for the bulkier naphthylmethyl

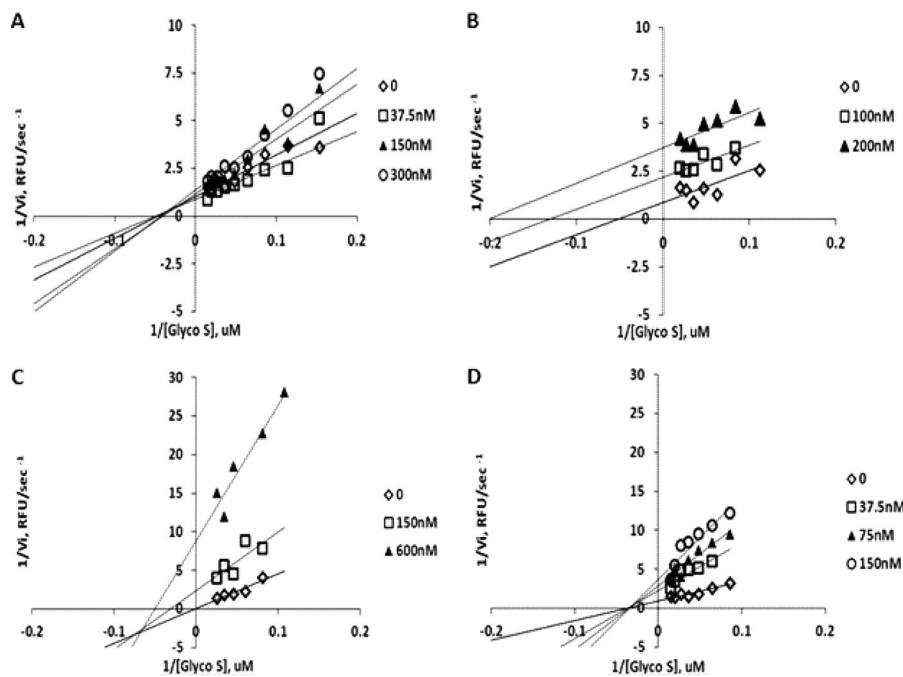


FIGURE 7. Lineweaver-Burk plots of glycosylated substrate hydrolysis by ADAM17 in the presence of representative members of library 1344. A, compound 24; B, compound 35; C, compound 61; D, compound 119.

in  $R_2$  yielded more potent compound 15 without the loss of selectivity. Interestingly, a similar substitution in compound 27 did not lead to the significant changes in activity or selectivity (Fig. 6, B and D, compounds 27 and 34). Similarly, substitution of the  $R_4$  2-adamantan-1-yl-ethyl group found in compounds 15 and 34 for cyclopentyl-methyl (compounds 17 and 36) resulted in unchanged potency and selectivity (Fig. 6, C–F).

Overall, individual compounds derived from the positional scan exhibited micromolar potency and good selectivity toward ADAM17. To our knowledge, there are no reports of ADAM17 inhibitors that spare ADAM10, MMP-8, and MMP-14. One of the most promising ADAM inhibitors that is currently in clinical trial for breast cancer, INCB7839 (Incyte Corp., Wilmington, DE), inhibits multiple metalloproteases (69), including equipotent low nanomolar range activity against both ADAM10 and -17.

**Inhibition Kinetics**—To interrogate the mechanism of inhibition for the most selective and potent libraries, inhibition kinetic studies were performed with samples  $R_1$ -24,  $R_2$ -35,  $R_3$ -61, and  $R_4$ -119. Non-linear regression analysis suggested pure non-competitive inhibition mechanisms for samples  $R_1$ -24,  $R_3$ -61, and  $R_4$ -119 ( $K_i/K_i' = 1.1 \pm 1.2$ ,  $0.91 \pm 2.5$ , and  $0.79 \pm 0.52$ , respectively), and an uncompetitive mechanism for  $R_2$ -35 ( $K_i/K_i' = 0.1 \pm 0.3$ ). Additional evaluation of inhibition mechanisms by the model comparison routine of GraphPad Prism software indicated that these are indeed preferred inhibition models. Examination of the kinetic data by a linearized Lineweaver-Burk graphic confirmed the pure non-competitive inhibition modality for  $R_1$ -24 and  $R_4$ -119 (Fig. 7, A and D) and uncompetitive modality for  $R_2$ -35 (Fig. 7B). In the case of  $R_3$ -61, the Lineweaver-Burk plot is suggestive of mixed inhibition (Fig. 7C) with elements of uncompetitive inhibition.

Most ADAM17 inhibitors described in the literature act via zinc binding due to the presence of zinc-binding moieties (e.g. hydroxamates, phosphinates) in their structures (5, 8, 61, 70).

The prominent feature of the basic scaffold of library 1344 (Fig. 3C) is two piperazine-2,3-dione moieties. Piperazine- and diketo-piperazine-based MMP and ADAM inhibitors have been described in the literature; however, they also have other zinc-binding groups present and as a consequence have broad inhibition profiles (71, 72). The piperazine group was shown to interact with catalytic zinc of farnesyl protein transferase via the nitrogen atom (73). Piperazine derivatives have not been co-crystallized with ADAM17; therefore, it is unknown whether piperazine moieties can contribute to the interactions with zinc of an ADAM17 active site. However, the prevalence of non- and uncompetitive inhibition modalities among selective ADAM17 inhibitors suggests that this chemotype acts via a non-zinc-binding mechanism, possibly by binding outside of the ADAM17 active site. In order to investigate this possibility, we performed dual inhibition kinetics using *N*-hydroxyacetamide (AHA) (Fig. 8A), a known zinc binder and competitive millimolar range inhibitor of many metalloproteases, in combination with inhibitor compound 15, following a methodology described previously (74). AHA was used in the concentration range of 0–2.5 mM, in combination with compound 15 at concentrations between 0 and 7.5  $\mu$ M. When initial velocities from this experiment were organized in a Yonetani-Theorell plot, they formed a series of intersecting lines of best fit (Fig. 8B). In Yonetani-Theorell plots, the intersecting lines suggest simultaneous (i.e. mutually non-exclusive) binding of both inhibitors to the enzyme (49). Because AHA is known to bind to zinc, compound 15 most likely acts via a non-zinc-binding mechanism and, potentially, outside of the active site and beyond the catalytic domain, as suggested by a recent report (33). Single inhibition kinetics of compound 15 suggest non-competitive inhibition ( $K_i/K_i' = 0.5 \pm 0.6$ ; Fig. 8C) consistent with mutually non-exclusive AHA binding. We investigated the possibility of compound 15 binding outside of the catalytic domain by

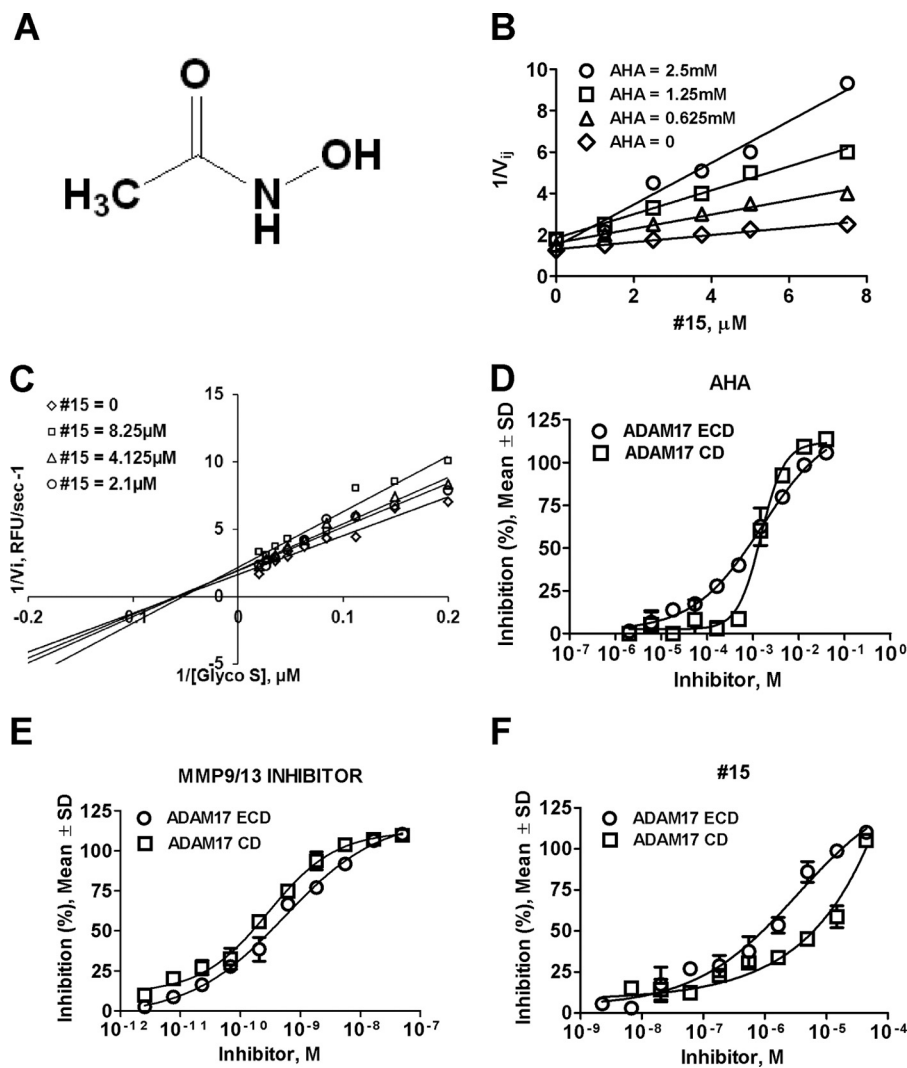


FIGURE 8. **Characterization of mechanism of inhibition of ADAM17 catalytic domain and ectodomain by compound 15.** A, structure of AHA; B, Yonetani-Theorell plot of glycosylated substrate hydrolysis by ADAM17 in the presence of AHA and compound 15. Note the *non-parallel lines* of best fit, indicating mutually non-exclusive binding by two inhibitors. C, Lineweaver-Burk plot of glycosylated substrate hydrolysis by ADAM17 in the presence of compound 15. Shown is a dose-response study of inhibition of ADAM17 catalytic domain and ectodomain by AHA (D), MMP-9/-13 inhibitor (E), and compound 15 (F). CD, catalytic domain-only.

performing dose-response experiments with compound 15 against ADAM17 ectodomain (ECD) and catalytic domain-only constructs. AHA and MMP-9/-13 inhibitor were utilized as controls. Both controls exhibited nearly identical  $IC_{50}$  values for inhibition of either construct (AHA  $IC_{50} = 1.5 \pm 0.2$  mM versus  $1.6 \pm 0.2$  mM for ADAM17 ECD and catalytic domain-only, respectively; MMP-9/-13 inhibitor  $IC_{50} = 0.3 \pm 0.03$  nM versus  $0.5 \pm 0.04$  nM for ADAM17 ECD and catalytic domain-only (CD), respectively; Fig. 8, D and E), whereas compound 15 inhibited ADAM17 ECD 10-fold more potently (compound 15  $IC_{50} = 4.2 \pm 0.4$   $\mu$ M versus  $47 \pm 4$   $\mu$ M for ADAM17 ECD and catalytic domain-only (CD), respectively; Fig. 8F). This suggests certain cooperativity between catalytic and non-catalytic domains of ADAM17 in the binding of compound 15. One possibility is that compound 15 can bind across domains due to the spatial proximity of the non-catalytic and catalytic domains, as described in the case of the inhibitory antibody reported by Tape *et al.* (33). The existence of a binding pocket within the catalytic domain capable of accommodating compound 15,

whose size is affected by the presence of a non-catalytic domain, is yet another possibility. The small size of compound 15, as compared with an antibody, makes the latter model more likely. Further structural studies are needed to ascertain the exact ADAM17 binding site of these novel, selective ADAM17 inhibitors.

**Significance**—Selective inhibitors of ADAM proteases can be useful research and therapeutic tools to study the roles of individual ADAM isoforms in diseases and normalcy. ADAM inhibitors reported to date act via active site zinc chelation and as a result inhibit multiple related zinc proteases (MMPs, ADAMs, and ADAMTSs). Here we report the discovery of a novel class of ADAM17-selective inhibitors that act via a non-zinc-binding mechanism.

This discovery was enabled by the development of a glycosylated, potentially exosite-binding substrate. Differences in the abilities of ADAM proteases to accommodate substrate carbohydrates point to the existence of unique exosites within ADAM structures that can be explored for discovery of iso-

form-selective non-zinc-binding inhibitors. These inhibitors were also able to inhibit ADAM17 hydrolysis of various non-glycosylated substrates (data not shown), suggesting their potential usefulness for a variety of applications that require ADAM17 inhibition.

Most cell surface proteins are glycosylated in one or more positions. Types of carbohydrate moieties present on the same cell surface protein can vary in disease and normalcy and thus can potentially be used as disease biomarkers. Results presented here suggest that differential glycosylation of substrates affects not only the rate of their hydrolysis but also the cleavage sites by different enzymes, which may lead to a release of different neopeptides in disease and normalcy.

## REFERENCES

- Houghten, R. A., Pinilla, C., Giulianotti, M. A., Appel, J. R., Dooley, C. T., Nefzi, A., Ostresh, J. M., Yu, Y., Maggiora, G. M., Medina-Franco, J. L., Brunner, D., and Schneider, J. (2008) Strategies for the use of mixture-based synthetic combinatorial libraries. Scaffold ranking, direct testing *in vivo*, and enhanced deconvolution by computational methods. *J. Comb. Chem.* **10**, 3–19
- Pinilla, C., Appel, J. R., Borràs, E., and Houghten, R. A. (2003) Advances in the use of synthetic combinatorial chemistry. Mixture-based libraries. *Nat. Med.* **9**, 118–122
- Moss, M. L., Stoeck, A., Yan, W., and Dempsey, P. J. (2008) ADAM10 as a target for anti-cancer therapy. *Curr. Pharm. Biotechnol.* **9**, 2–8
- Kataoka, H. (2009) EGFR ligands and their signaling scissors, ADAMs, as new molecular targets for anticancer treatments. *J. Dermatol. Sci.* **56**, 148–153
- Moss, M. L., Sklair-Tavron, L., and Nudelman, R. (2008) Drug insight. Tumor necrosis factor-converting enzyme as a pharmaceutical target for rheumatoid arthritis. *Nat. Clin. Pract. Rheumatol.* **4**, 300–309
- Asai, M., Hattori, C., Szabó, B., Sasagawa, N., Maruyama, K., Tanuma, S., and Ishiura, S. (2003) Putative function of ADAM9, ADAM10, and ADAM17 as APP  $\alpha$ -secretase. *Biochem. Biophys. Res. Commun.* **301**, 231–235
- Kenny, P. A., and Bissell, M. J. (2007) Targeting TACE-dependent EGFR ligand shedding in breast cancer. *J. Clin. Invest.* **117**, 337–345
- Georgiadis, D., and Yiotakis, A. (2008) Specific targeting of metzincin family members with small-molecule inhibitors. Progress toward a multifarious challenge. *Bioorg. Med. Chem.* **16**, 8781–8794
- Edwards, D. R., Handsley, M. M., and Pennington, C. J. (2008) The ADAM metalloproteinases. *Mol. Aspects Med.* **29**, 258–289
- Fingleton, B. (2007) Matrix metalloproteinases as valid clinical targets. *Curr. Pharm. Des.* **13**, 333–346
- Dennis, M. S., Eigenbrot, C., Skelton, N. J., Ultsch, M. H., Santell, L., Dwyer, M. A., O'Connell, M. P., and Lazarus, R. A. (2000) Peptide exosite inhibitors of factor VIIa as anticoagulants. *Nature* **404**, 465–470
- Roberge, M., Peek, M., Kirchofer, D., Dennis, M. S., and Lazarus, R. A. (2002) Fusion of two distinct peptide exosite inhibitors of Factor VIIa. *Biochem. J.* **363**, 387–393
- Roberge, M., Santell, L., Dennis, M. S., Eigenbrot, C., Dwyer, M. A., and Lazarus, R. A. (2001) A novel exosite on coagulation factor VIIa and its molecular interactions with a new class of peptide inhibitors. *Biochemistry* **40**, 9522–9531
- Izaguirre, G., Rezaie, A. R., and Olson, S. T. (2009) Engineering functional antithrombin exosites in  $\alpha$ 1-proteinase inhibitor that specifically promote the inhibition of factor Xa and factor IXa. *J. Biol. Chem.* **284**, 1550–1558
- Scheer, J. M., Romanowski, M. J., and Wells, J. A. (2006) A common allosteric site and mechanism in caspases. *Proc. Natl. Acad. Sci. U.S.A.* **103**, 7595–7600
- Hosseini, M., Jiang, L., Sørensen, H. P., Jensen, J. K., Christensen, A., Fogh, S., Yuan, C., Andersen, L. M., Huang, M., Andreason, P. A., and Jensen, K. J. (2011) Elucidation of the contribution of active site and exosite interactions to affinity and specificity of peptidyl serine protease inhibitors, using non-natural arginine analogs. *Mol. Pharmacol.* **80**, 585–597
- Johnson, A. R., Pavlovsky, A. G., Ortwine, D. F., Prior, F., Man, C. F., Bornemeier, D. A., Banotai, C. A., Mueller, W. T., McConnell, P., Yan, C., Baragi, V., Lesch, C., Roark, W. H., Wilson, M., Datta, K., Guzman, R., Han, H. K., and Dyer, R. D. (2007) Discovery and characterization of a novel inhibitor of matrix metalloprotease-13 that reduces cartilage damage *in vivo* without joint fibroplasia side effects. *J. Biol. Chem.* **282**, 27781–27791
- Engel, C. K., Pirard, B., Schimanski, S., Kirsch, R., Habermann, J., Klingler, O., Schlotte, V., Weithmann, K. U., and Wendt, K. U. (2005) Structural basis for the highly selective inhibition of MMP-13. *Chem. Biol.* **12**, 181–189
- Baragi, V. M., Becher, G., Bendele, A. M., Biesinger, R., Bluhm, H., Boer, J., Deng, H., Dodd, R., Essers, M., Feuerstein, T., Gallagher, B. M., Jr., Gege, C., Hochgurtel, M., Hofmann, M., Jaworski, A., Jin, L., Kiely, A., Korniski, B., Kroth, H., Nix, D., Nolte, B., Piecha, D., Powers, T. S., Richter, F., Schneider, M., Steeneck, C., Sucholeiki, I., Taveras, A., Timmermann, A., Van Veldhuizen, J., Weik, J., Wu, X., and Xia, B. (2009) A new class of potent matrix metalloproteinase 13 inhibitors for potential treatment of osteoarthritis. Evidence of histologic and clinical efficacy without musculoskeletal toxicity in rat models. *Arthritis Rheum.* **60**, 2008–2018
- Lauer-Fields, J. L., Minond, D., Chase, P. S., Baillargeon, P. E., Saldanha, S. A., Stawikowska, R., Hodder, P., and Fields, G. B. (2009) High throughput screening of potentially selective MMP-13 exosite inhibitors utilizing a triple-helical FRET substrate. *Bioorg. Med. Chem.* **17**, 990–1005
- Roth, J., Minond, D., Darout, E., Liu, Q., Lauer, J., Hodder, P., Fields, G. B., and Roush, W. R. (2011) Identification of novel, exosite-binding matrix metalloproteinase-13 inhibitor scaffolds. *Bioorg. Med. Chem. Lett.* **21**, 7180–7184
- Wittwer, A. J., Hills, R. L., Keith, R. H., Munie, G. E., Arner, E. C., Anglin, C. P., Malfait, A. M., and Tortorella, M. D. (2007) Substrate-dependent inhibition kinetics of an active site-directed inhibitor of ADAMTS-4 (aggrecanase 1). *Biochemistry* **46**, 6393–6401
- Yegneswaran, S., Tiefenbrunn, T. K., Fernandez, J. A., and Dawson, P. E. (2007) Manipulation of thrombin exosite I, by ligand-directed covalent modification. *J. Thromb. Haemost.* **5**, 2062–2069
- Sela-Passwell, N., Rosenblum, G., Shoham, T., and Sagi, I. (2010) Structural and functional bases for allosteric control of MMP activities. Can it pave the path for selective inhibition? *Biochim. Biophys. Acta* **1803**, 29–38
- Rzychon, M., Chmiel, D., and Stec-Niemczyk, J. (2004) Modes of inhibition of cysteine proteases. *Acta Biochim. Pol.* **51**, 861–873
- Ishii, R., Minagawa, A., Takaku, H., Takagi, M., Nashimoto, M., and Yokoyama, S. (2007) The structure of the flexible arm of *Thermotoga maritima* tRNase Z differs from those of homologous enzymes. *Acta Crystallogr. Sect. F Struct. Biol. Cryst. Commun.* **63**, 637–641
- Prudent, R., Sautel, C. F., and Cochet, C. (2010) Structure-based discovery of small molecules targeting different surfaces of protein-kinase CK2. *Biochim. Biophys. Acta* **1804**, 493–498
- Pantke, M. M., Reif, A., Valtschanoff, J. G., Shutenko, Z., Frey, A., Weinberg, R. J., Pfeleiderer, W., and Schmidt, H. H. (2001) Pterin interactions with distinct reductase activities of NO synthase. *Biochem. J.* **356**, 43–51
- Vogel, A., Schilling, O., Späth, B., and Marchfelder, A. (2005) The tRNase Z family of proteins. Physiological functions, substrate specificity, and structural properties. *Biol. Chem.* **386**, 1253–1264
- Gurard-Levin, Z. A., and Mrksich, M. (2008) The activity of HDAC8 depends on local and distal sequences of its peptide substrates. *Biochemistry* **47**, 6242–6250
- Takeda, S., Igarashi, T., and Mori, H. (2007) Crystal structure of RVV-X. An example of evolutionary gain of specificity by ADAM proteinases. *FEBS Lett.* **581**, 5859–5864
- Hall, T., Pegg, L. E., Pauley, A. M., Fischer, H. D., Tomasselli, A. G., and Zack, M. D. (2009) ADAM8 substrate specificity. Influence of pH on pre-processing and proteoglycan degradation. *Arch. Biochem. Biophys.* **491**, 106–111
- Tape, C. J., Willems, S. H., Dombernowsky, S. L., Stanley, P. L., Fogarasi, M., Ouwehand, W., McCafferty, J., and Murphy, G. (2011) Cross-domain inhibition of TACE ectodomain. *Proc. Natl. Acad. Sci. U.S.A.* **108**, 5578–5583

34. Lauer-Fields, J. L., Minond, D., Sritharan, T., Kashiwagi, M., Nagase, H., and Fields, G. B. (2007) Substrate conformation modulates aggrecanase (ADAMTS-4) affinity and sequence specificity. Suggestion of a common topological specificity for functionally diverse proteases. *J. Biol. Chem.* **282**, 142–150
35. Minond, D., Lauer-Fields, J. L., Cudic, M., Overall, C. M., Pei, D., Brew, K., Moss, M. L., and Fields, G. B. (2007) Differentiation of secreted and membrane-type matrix metalloproteinase activities based on substitutions and interruptions of triple-helical sequences. *Biochemistry* **46**, 3724–3733
36. Minond, D., Lauer-Fields, J. L., Cudic, M., Overall, C. M., Pei, D., Brew, K., Visse, R., Nagase, H., and Fields, G. B. (2006) The roles of substrate thermal stability and P2 and P1' subsite identity on matrix metalloproteinase triple-helical peptidase activity and collagen specificity. *J. Biol. Chem.* **281**, 38302–38313
37. Minond, D., Lauer-Fields, J. L., Nagase, H., and Fields, G. B. (2004) Matrix metalloproteinase triple-helical peptidase activities are differentially regulated by substrate stability. *Biochemistry* **43**, 11474–11481
38. Caescu, C. I., Jeschke, G. R., and Turk, B. E. (2009) Active-site determinants of substrate recognition by the metalloproteinases TACE and ADAM10. *Biochem. J.* **424**, 79–88
39. Moss, M. L., and Rasmussen, F. H. (2007) Fluorescent substrates for the proteinases ADAM17, ADAM10, ADAM8, and ADAM12 useful for high-throughput inhibitor screening. *Anal. Biochem.* **366**, 144–148
40. Moss, M. L., Rasmussen, F. H., Nudelman, R., Dempsey, P. J., and Williams, J. (2010) Fluorescent substrates useful as high-throughput screening tools for ADAM9. *Comb. Chem. High Throughput Screen.* **13**, 358–365
41. Imperiali, B., and Rickert, K. W. (1995) Conformational implications of asparagine-linked glycosylation. *Proc. Natl. Acad. Sci. U.S.A.* **92**, 97–101
42. Otvos, L., Jr., and Cudic, M. (2003) Conformation of glycopeptides. *Mini Rev. Med. Chem.* **3**, 703–711
43. Bann, J. G., Peyton, D. H., and Bächinger, H. P. (2000) Sweet is stable: glycosylation stabilizes collagen. *FEBS Lett.* **473**, 237–240
44. Tagashira, M., Iijima, H., Isogai, Y., Hori, M., Takamatsu, S., Fujibayashi, Y., Yoshizawa-Kumagaya, K., Isaka, S., Nakajima, K., Yamamoto, T., Teshima, T., and Toma, K. (2001) Site-dependent effect of O-glycosylation on the conformation and biological activity of calcitonin. *Biochemistry* **40**, 11090–11095
45. Meldal, M., and Bock, K. (1994) A general approach to the synthesis of O- and N-linked glycopeptides. *Glycoconj. J.* **11**, 59–63
46. Takakura-Yamamoto, R., Yamamoto, S., Fukuda, S., and Kurimoto, M. (1996) O-Glycosylated species of natural human tumor necrosis factor- $\alpha$ . *Eur. J. Biochem.* **235**, 431–437
47. Bringman, T. S., Lindquist, P. B., and Derynck, R. (1987) Different transforming growth factor- $\alpha$  species are derived from a glycosylated and palmitoylated transmembrane precursor. *Cell* **48**, 429–440
48. Wollscheid, B., Bausch-Fluck, D., Henderson, C., O'Brien, R., Bibel, M., Schiess, R., Aebersold, R., and Watts, J. D. (2009) Mass spectrometric identification and relative quantification of N-linked cell surface glycoproteins. *Nat. Biotechnol.* **27**, 378–386
49. Martinez-Irujo, J. J., Villahermosa, M. L., Mercapide, J., Cabodevilla, J. F., and Santiago, E. (1998) Analysis of the combined effect of two linear inhibitors on a single enzyme. *Biochem. J.* **329**, 689–698
50. Copeland, R. (2000) *Enzymes*, 2nd Ed., pp. 289–290, Wiley-VCH, New York
51. Chalaris, A., Garbers, C., Rabe, B., Rose-John, S., and Scheller, J. (2011) The soluble interleukin 6 receptor. Generation and role in inflammation and cancer. *Eur. J. Cell Biol.* **90**, 484–494
52. Müllberg, J., Oberthür, W., Lottspeich, F., Mehl, E., Dittrich, E., Graeve, L., Heinrich, P. C., and Rose-John, S. (1994) The soluble human IL-6 receptor. Mutational characterization of the proteolytic cleavage site. *J. Immunol.* **152**, 4958–4968
53. Cole, A. R., Hall, N. E., Treutlein, H. R., Eddes, J. S., Reid, G. E., Moritz, R. L., and Simpson, R. J. (1999) Disulfide bond structure and N-glycosylation sites of the extracellular domain of the human interleukin-6 receptor. *J. Biol. Chem.* **274**, 7207–7215
54. Wormald, M. R., Petrescu, A. J., Pao, Y. L., Glithero, A., Elliott, T., and Dwek, R. A. (2002) Conformational studies of oligosaccharides and glycopeptides. Complementarity of NMR, x-ray crystallography, and molecular modeling. *Chem. Rev.* **102**, 371–386
55. McManus, A. M., Otvos, L., Jr., Hoffmann, R., and Craik, D. J. (1999) Conformational studies by NMR of the antimicrobial peptide, drosocin, and its non-glycosylated derivative. Effects of glycosylation on solution conformation. *Biochemistry* **38**, 705–714
56. Falenski, J. A., Gerling, U. L., and Kokschi, B. (2010) Multiple glycosylation of *de novo* designed  $\alpha$ -helical coiled coil peptides. *Bioorg. Med. Chem.* **18**, 3703–3706
57. Zhao, Y. H., Abraham, M. H., and Zissimos, A. M. (2003) Fast calculation of van der Waals volume as a sum of atomic and bond contributions and its application to drug compounds. *J. Org. Chem.* **68**, 7368–7373
58. Patel, I. R., Attur, M. G., Patel, R. N., Stuchin, S. A., Abagyan, R. A., Abramson, S. B., and Amin, A. R. (1998) TNF- $\alpha$  convertase enzyme from human arthritis-affected cartilage. Isolation of cDNA by differential display, expression of the active enzyme, and regulation of TNF- $\alpha$ . *J. Immunol.* **160**, 4570–4579
59. Huang, A., Joseph-McCarthy, D., Lovering, F., Sun, L., Wang, W., Xu, W., Zhu, Y., Cui, J., Zhang, Y., and Levin, J. I. (2007) Structure-based design of TACE selective inhibitors. Manipulations in the S1'–S3' pocket. *Bioorg. Med. Chem.* **15**, 6170–6181
60. Healy, E. F., Romano, P., Mejia, M., and Lindfors, G., 3rd. (2010) Acetylenic inhibitors of ADAM10 and ADAM17. *In silico* analysis of potency and selectivity. *J. Mol. Graph. Model.* **29**, 436–442
61. Bahia, M. S., and Silakari, O. (2010) Tumor necrosis factor  $\alpha$ -converting enzyme. An encouraging target for various inflammatory disorders. *Chem. Biol. Drug Des.* **75**, 415–443
62. Houghten, R. A., Pinilla, C., Appel, J. R., Blondelle, S. E., Dooley, C. T., Eichler, J., Nefzi, A., and Ostresh, J. M. (1999) Mixture-based synthetic combinatorial libraries. *J. Med. Chem.* **42**, 3743–3778
63. Balbín, M., Fueyo, A., Tester, A. M., Pendás, A. M., Pitiot, A. S., Astudillo, A., Overall, C. M., Shapiro, S. D., and López-Otin, C. (2003) Loss of collagenase-2 confers increased skin tumor susceptibility to male mice. *Nat. Genet.* **35**, 252–257
64. Palavalli, L. H., Prickett, T. D., Wunderlich, J. R., Wei, X., Burrell, A. S., Porter-Gill, P., Davis, S., Wang, C., Cronin, J. C., Agrawal, N. S., Lin, J. C., Westbroek, W., Hoogstraten-Miller, S., Molinolo, A. A., Fetsch, P., Filie, A. C., O'Connell, M. P., Banister, C. E., Howard, J. D., Buckhaults, P., Weeraratna, A. T., Brody, L. C., Rosenberg, S. A., and Samuels, Y. (2009) Analysis of the matrix metalloproteinase family reveals that MMP8 is often mutated in melanoma. *Nat. Genet.* **41**, 518–520
65. Szabova, L., Chrysovergis, K., Yamada, S. S., and Holmbeck, K. (2008) MT1-MMP is required for efficient tumor dissemination in experimental metastatic disease. *Oncogene* **27**, 3274–3281
66. Wang, Z., Herzog, C., Kaushal, G. P., Gokden, N., and Mayeux, P. R. (2011) Actinonin, a meprin A inhibitor, protects the renal microcirculation during sepsis. *Shock* **35**, 141–147
67. Becker-Pauly, C., Bruns, B. C., Damm, O., Schütte, A., Hammouti, K., Burmester, T., and Stöcker, W. (2009) News from an ancient world. Two novel astacin metalloproteases from the horseshoe crab. *J. Mol. Biol.* **385**, 236–248
68. Santos, R. G., Giulianotti, M. A., Dooley, C. T., Pinilla, C., Appel, J. R., and Houghten, R. A. (2011) Use and implications of the harmonic mean model on mixtures for basic research and drug discovery. *ACS Comb. Sci.* **13**, 337–344
69. Witters, L., Scherle, P., Friedman, S., Fridman, J., Caulder, E., Newton, R., and Lipton, A. (2008) Synergistic inhibition with a dual epidermal growth factor receptor/HER-2/neu tyrosine kinase inhibitor and a disintegrin and metalloprotease inhibitor. *Cancer Res.* **68**, 7083–7089
70. Murumkar, P. R., DasGupta, S., Chandani, S. R., Giridhar, R., and Yadav, M. R. (2010) Novel TACE inhibitors in drug discovery. A review of patented compounds. *Expert Opin. Ther. Pat.* **20**, 31–57
71. Letavic, M. A., Barberia, J. T., Carty, T. J., Hardink, J. R., Liras, J., Lopresti-Morrow, L. L., Mitchell, P. G., Noe, M. C., Reeves, L. M., Snow, S. L., Stam, E. J., Sweeney, F. J., Vaughn, M. L., and Yu, C. H. (2003) Synthesis and biological activity of piperazine-based dual MMP-13 and TNF- $\alpha$ -converting enzyme inhibitors. *Bioorg. Med. Chem. Lett.* **13**, 3243–3246

72. Szardenings, A. K., Antonenko, V., Campbell, D. A., DeFrancisco, N., Ida, S., Shi, L., Sharkov, N., Tien, D., Wang, Y., and Navre, M. (1999) Identification of highly selective inhibitors of collagenase-1 from combinatorial libraries of diketopiperazines. *J. Med. Chem.* **42**, 1348–1357
73. Njoroge, F. G., Vibulbhan, B., Pinto, P., Strickland, C., Bishop, W. R., Nomeir, A., and Girijavallabhan, V. (2006) Enhanced FTase activity achieved via piperazine interaction with catalytic zinc. *Bioorg. Med. Chem. Lett.* **16**, 984–988
74. Gooljarsingh, L. T., Lakdawala, A., Coppo, F., Luo, L., Fields, G. B., Tummino, P. J., and Gontarek, R. R. (2008) Characterization of an exosite binding inhibitor of matrix metalloproteinase 13. *Protein Sci.* **17**, 66–71